

A remarkable long-term light curve, and deep, low-state spectroscopy: *Swift* & *XMM-Newton* monitoring of the NLS1 galaxy Mkn 335

Dirk Grupe¹, S. Komossa^{2,3,4}, Luigi C. Gallo⁵, Anna Lia Longinotti^{6,7}, Andrew C. Fabian⁸, Anil K. Pradhan⁹, Michael Gruberbauer⁵, Dawei Xu¹⁰

ABSTRACT

The Narrow-line Seyfert 1 galaxy (NLS1) Mkn 335 is remarkable because it has repeatedly shown deep, long X-ray low-states which show pronounced spectral structure. It has become one of the prototype AGN in deep minimum X-ray states. Here we report on the continuation of our ongoing monitoring campaign with *Swift* and the examination of the low state X-ray spectra based on a 200 ks triggered observation with *XMM-Newton* in June 2009. *Swift* has continuously monitored Mkn 335 since May 2007 typically on a monthly basis. This is one of the longest simultaneous UV/X-ray light curves so far obtained for an active galactic nucleus (AGN). Mkn 335 has shown strong X-ray variability even on time scales of hours. In the UV, it turns out to be one of the most variable among NLS1s. Long-term *Swift* monitoring allow us to examine correlations between the UV, X-rays and X-ray hardness ratios. We find no significant correlation or lag between the UV and X-ray variability; however, we do find distinct trends in the behavior of the hardness ratio variability. The hardness ratio and count rate are correlated in the low-flux state, but no correlation is seen in the high-state. The X-ray low-state spectra of the 2007 and 2009 *XMM-Newton* observations display significant spectral variability. We fit the X-ray spectra with a suite of phenomenological models in order to characterize the data. The broad band CCD spectrum can be fitted equally well with partial absorption and blurred reflection models. These more complicated models are explored in further detail in upcoming work.

Subject headings: galaxies: active, galaxies: individual (Mkn 335), galaxies: Seyferts, X-rays: galaxies

¹Department of Astronomy and Astrophysics, Pennsylvania State University, 525 Davey Lab, University Park, PA 16802; grupe@astro.psu.edu

²Technische Universität München, Fakultät für Physik, James-Franck-Strasse 1/I, D-85748 Garching, Germany; stefanie.komossa@gmx.de

³Excellence Cluster Universe, TUM, Boltzmannstrasse 2, 85748 Garching, Germany

⁴Max Planck Institut für Plasmaphysik, Boltzmannstrasse 2, 85748 Garching, Germany

⁵Department of Astronomy and Physics, Saint Mary's University, Halifax, NS B3H 3C3, Canada; lgallo@ap.stmarys.ca

⁶MIT Kavli Institute for Astrophysics and Space Research 77 Massachusetts Avenue, NE80-6011 Cambridge, MA 02139

⁷XMM-Newton Science Operations Centre ESAC, P.O. Box 78 28691 Villanueva de la Cañada, Madrid, Spain

⁸Institute of Astronomy, Madingley Road, Cambridge,

1. Introduction

While AGN typically vary in X-rays by factors of a few (e.g. Grupe et al. 2001), some AGN show dramatic drops in their X-ray flux, accompanied by changes in their spectrum. These AGN are known to be typically X-ray bright, but for some time they display very low flux states which makes them different from AGN such as PHL 1811 which are intrinsically X-ray weak (Leighly et al. 2007).

CB3 0HA, UK

⁹Department of Astronomy, The Ohio State University, 140 W 18th Av, Columbus, OH; pradhan@astronomy.ohio-state.edu

¹⁰National Astronomical Observatories, Chinese Academy of Sciences, 20A Datun Road, Beijing 100012, China; dwxu@nao.cas.cn

Some recent examples of such deep minimum states observed in AGN are PG 2112+059, PG 1535+547, PG 1543+489, RX J2217.9–5941, Mkn 335, PHL 1092, and PG 0844+349 (Schartel et al. 2010, 2007; Ballo et al. 2008; Vignali et al. 2008; Grupe et al. 2004a; Grupe et al. 2007b, 2008a; Miniutti et al. 2009; Gallo et al. 2011). Absorption has always been considered to play an important role in explaining AGN X-ray spectra. Variability through a variable absorber may play a much more important role in AGN than previously thought (e.g. Turner & Miller 2009). Some of the best examples of variable absorbers are e.g. NGC 1365 (Risaliti et al. 2009), Mkn 766 (Miller et al. 2007; Turner et al. 2007), 1 H0557–385 (Longinotti et al. 2009), and NGC 3516 Turner et al. (2011).

However, this picture is far from being complete and clear. Besides absorption, a popular explanation of the X-ray low states in AGN are reflection models such as proposed by Fabian et al. (2002, 2004, 2009) for 1H 0707-495, or by Gallo (2006) for NLS1s in general. Both, reflection and partial covering absorber models produce relatively similar X-ray spectra (see e.g. discussion in Grupe et al. 2008a). To make things even more complex, as shown by e.g. Chevalier et al. (2006) and Merloni et al. (2006), the X-ray spectrum can be dominated in the high state by reflection and is then modified by a partial covering absorber when the AGN is in a low state. Even for MCG-6-30-15, which has been the poster-child for reflection models after the ASCA detection of a broad red wing of the Fe $K\alpha$ line by Tanaka et al. (1995), Miller et al. (2008, 2009) argued that its X-ray spectra can be consistently explained by partial covering absorption.

Bright AGN in deep low-states with well-covered light curves and good low-state spectra are essential for further exploring the physics which are responsible for the structures and features seen in AGN X-ray spectra, and especially in low-states, where spectral complexity is most pronounced. The NLS1 Mkn 335 ($\alpha_{2000} = 00^{\text{h}}06^{\text{m}}19.^{\text{s}}5$, $\delta_{2000} = +20^{\circ}12'11''.0$) is such an AGN: it goes repeatedly into deep low-states, is relatively X-ray bright even in those states, and has been monitored by us for years to identify these low-states. It shows interesting spectral structures, and one possible interpretation has

been that it exhibits an unusually broad Fe line (Longinotti et al. 2007a). It is nearby ($z=0.0258$), well studied in the optical spectral band, and has a well-measured BH mass of $1.4 \times 10^7 M_{\odot}$ from reverberation mapping (Peterson et al. 2004; Grier et al. 2012).

Mkn 335 has been known to be an X-ray bright AGN for decades, starting with UHURU (Tananbaum et al. 1978) and EINSTEIN (Halpern 1982). EXOSAT and BBXRT observations suggested a strong soft X-ray excess in the X-ray spectrum of Mkn 335 (Pounds et al. 1987; Turner et al. 1993, respectively) while Nandra & Pounds (1994) reported on the presence of a warm absorber in this source. During the ROSAT All Sky-Survey and pointed observations Mkn 335 appeared to be X-ray bright, and was modeled with a strong soft X-ray excess (Grupe et al. 2001). From the 1993 observations by ASCA (George et al. 2000), Leighly (1999) concluded that the X-ray spectrum was affected by the presence of a warm absorber, while Ballantyne et al. (2001) interpreted the spectral shape by X-ray reflection on the accretion disk. Mkn 335 was also observed by *XMM-Newton* in 2000 and 2006 (Gondoin et al. 2002; Longinotti et al. 2007a; Longinotti et al. 2007; O’Neill et al. 2007; Arevalo et al. 2008) and *Suzaku* in June 2006 (Larsson et al. 2008). In all cases Mkn 335 was X-ray bright, with the exception of one EXOSAT observation in 1983 (Pounds et al. 1987).

However, when Mkn 335 was observed by *Swift* (Gehrels et al. 2004) in 2007 May as part of a *Swift* fill in project to study the spectral energy distributions in AGN (Grupe et al. 2010) it appeared to be dramatically fainter in X-rays than expected from previous X-ray observations (Grupe et al. 2007b). In order to investigate the nature of the low-state in more detail we initiated a Target-of-Opportunity (ToO) observation with *XMM-Newton*, which was executed on 2007 July 10 (Grupe et al. 2008a). During this 22 ks *XMM-Newton* observation we discovered strong soft X-ray emission lines of H and He-like ions such as OVII (Grupe et al. 2008a; Longinotti et al. 2008) in the Reflection Grating Spectrometer (RGS; den Herder et al. 2001). These lines are only visible during an extreme X-ray low-state and they can provide information of the physical conditions of the gas surrounding the central black

hole. Because the 22ks *XMM-Newton* observation was too short to obtain any reliable line ratios, we applied for a 200ks *XMM-Newton* observation which would be triggered by a low state seen by *Swift*. When *Swift* started the monitoring campaign again in May 2009 after Mkn 335 came out of the sun constraint, it appeared to be again in an extreme low state. We therefore triggered our approved *XMM-Newton* observation and observed Mkn 335 for 200 ks in 2009 June 11th to 14th. Mkn 335 also became a target of our *Swift* Guest Investigator program in 2008 in which we monitored the AGN on a weekly basis in X-rays and all 6 UVOT filters.

Here we report on the results of the *Swift* monitoring campaign of Mkn 335 and the continuum short term light curve measured by *XMM-Newton* during the 200 ks triggered observation. This first paper in a sequence focusses on presenting the rich data sets, on simple modeling, and on revealing spectral trends. In-depth modeling of the multi-component warm absorber based on the RGS data, and a detailed investigation of blurred reflection models will each be presented in follow-up work. This Paper is organized as follows: in Section 2 we describe the observations and the data reduction of the *Swift* and *XMM-Newton* observations. In Section 3 we present the long- and short-term light curves and the analysis of the X-ray spectra obtained by *XMM-Newton*. The results of this analysis are discussed in Section 4. Throughout the paper spectral indices are denoted as energy spectral indices with $F_\nu \propto \nu^{-\alpha}$. Luminosities are calculated assuming a Λ CDM cosmology with $\Omega_M=0.27$, $\Omega_\Lambda=0.73$ and a Hubble constant of $H_0=75 \text{ km s}^{-1} \text{ Mpc}^{-1}$ corresponding to a luminosity distance $D=105 \text{ Mpc}$. All errors are 90% confidence unless stated otherwise.

2. Observations and data reduction

2.1. Swift observations

Swift started monitoring Mkn 335 on 2007 May 17 and still continues with this campaign on at least a monthly basis (Table 1), except for the period of February to May when Mkn 335 is in sun constraint for *Swift*. As part of a *Swift* Guest Investigator program the cadence was changed to once per week starting in June 2008. The X-Ray Telescope (XRT, Burrows et al. 2005) ob-

servations were performed in Photon Counting mode (PC mode Hill et al. 2004). X-ray data were reduced with the task *xrtpipeline* version 0.12.1. Source and background photons were extracted with *XSELECT* version 2.4, from circles with radii of $47''$ and $189''$, respectively when the source count rate was less than $0.4 \text{ counts s}^{-1}$. However, during some parts of our monitoring campaign the count rates were significantly higher than $0.4 \text{ counts s}^{-1}$ which means that the data were affected by pileup. In order to avoid the effects of pileup we excluded the inner part of the Point Spread Function, depending on the brightness of the AGN. The spectral data were re-binned with at least 20 photons per bin using *grppha* version 3.0.0. The 0.3-10.0 keV spectra were analyzed with *XSPEC* version 12.3.1x (Arnaud 1996). The auxiliary response files were created with *xrtmkarf* and corrected using the exposure maps, and the standard response matrices *swxpc0to12s0_20010101v011.rmf* and *swxpc0to12s6_20010101v011.rmf* were used for the observations before and after the XRT substrate voltage change in August 2007, respectively (Godet et al. 2009).

The UV-optical Telescope (UVOT, Roming et al. 2005) covers the range between $1700\text{-}6500\text{\AA}$ and is a sister instrument of *XMM-Newton*'s OM. Although it has a similar set of filters to the OM (Mason et al. 2001; Roming et al. 2005), the UVOT UV throughput is a factor of about 10 higher than that of the OM. The UVOT data were coadded for each segment in each filter with the UVOT task *uvotimsum* version 1.3. Source photons in all filters were selected in a circle with a radius of $5''$. UVOT magnitudes and fluxes were measured with the task *uvotsource* version 3 based on the most recent UVOT calibration as described in Poole et al. (2008) and Breeveld et al. (2010). The UVOT data were corrected for Galactic reddening ($E_{B-V} = 0.035$; Schlegel et al. 1998). The correction factor in each filter was calculated with equation (2) in Roming et al. (2009) who used the standard reddening correction curves by Cardelli et al. (1989).

2.2. XMM-Newton observations

We observed Mkn 335 with *XMM-Newton* (Jansen et al. 2001) on 2009 June 11 to 14 for a total of 200 ks split over orbits 1741 and

1742. A summary of the observations with each of the instruments on-board *XMM-Newton* is given in Table 2. The European Photon Imaging Camera (EPIC) pn (Strüder et al. 2001) was operated in Large Window mode with the thin filter. This combination was chosen to avoid pileup in case the AGN re-brightened. The two EPIC MOS (Turner et al. 2001) were both operated in Full-Frame mode with the medium filters. High-resolution X-ray spectroscopy was performed using the two Reflection Grating Spectrometers (RGS; den Herder et al. 2001) on-board *XMM-Newton*. Optical photometry was performed in 5 filters with the Optical Monitor (OM; Mason et al. 2001). The data are used to measure the optical-to-X-ray spectral energy distribution of Mkn 335 during the *XMM-Newton* observation. Due to slew problems at the beginning of the observations, V-filter observations were not obtained. All OM observations were performed in a science-user defined configuration with a $7' \times 7'$ observing window.

The *XMM-Newton* data were processed in the standard way using the XMMSAS version *xmmsas_20100423_1803-10.0.0*. The EPIC pn data were checked for episodes of high particle background. At the end of the first orbit (odsID 0600540601) the pn data were strongly affected by high particle background. Times with a background at energies $E > 10$ keV was larger than 10 counts s^{-1} were screened and not used for spectral analysis. This left an effective observing time of 99036s. During the second orbit (ObsID 0600540501) there were only very short episodes of high particle background. The total screened exposure time during this orbit was 69339s.

The source X-ray photons in the EPIC pn and MOS were selected in a circular region with a radius of $1'$. Likewise, background photons were selected from a nearby, source-free region with the same radius. Only single and double events (PATTERN.1e.4) and single to quadruple events (PATTERN.1e.12) were selected for the pn and MOS data, respectively. The spectra were rebinned with the XMMSAS task *specgroup* with an oversampling of 3 of the resolution elements at the energy of the bin. The redistribution matrices and the auxiliary response files were created by the XMMSAS tasks *rmfgen* and *arfgen*, respectively. We included also the 2007 *XMM-Newton* pn data

in our analysis. Note, however, that we also applied *specgroup* to rebin this spectrum and that the results may slightly differ from those presented in Grupe et al. (2008a). For comparison purposes, we also display the 2006 *XMM-Newton* high-state data in form of a light curve and hardness ratios.

RGS spectra and response matrices were created by the standard RGS XMMSAS tool *rgsproc*. The RGS spectra were rebinned with 10 photons per bin using *grppha*. Spectral fits to the EPIC pn and MOS, and RGS spectra were performed with XSPEC version 12.3.1x (Arnaud 1996). The OM data were processed with the XMMSAS task *omichain*. The magnitudes and fluxes of Mkn 335 were taken from the source lists created by the *omichain* task. For the count rate to flux conversion we used the conversion factors given in the OM Calibration document XMM-SOC-CAL-TN-0019.

2.3. Xinglong optical spectroscopy

The optical spectrum of Mkn 335 displays strong high-ionization iron coronal lines. In order to search for changes in the broad emission lines, and in the coronal lines, we have triggered an optical spectroscopic observation of Mkn 335 with the 2.16m Xinglong telescope quasi-simultaneous with the 2009 *XMM-Newton* observation.

The data were acquired on 2009 July 31 with the Opto-Mechanics Research (OMR) spectrograph equipped with a 600 line mm^{-1} grating and the $2''$ slit. This setup produces a resolution of 5\AA . The spectrum of Mrk 335 was taken with 3600s exposure.

Data reduction was done following standard procedures using IRAF. The CCD reductions included bias subtraction, flat-field correction, and cosmic-ray removal. Wavelength and flux calibration were performed.

We find that within the uncertainties there is no variability in the coronal lines, similar to our previous result (Grupe et al. 2008a).

3. Results

3.1. Long-term light curve observed by *Swift*

Figure 1 displays the *Swift* XRT count rate and hardness ratio light curves as well the the UVOT

light curves in each of the 6 filters. Note that after the end of the *Swift* GI program for Mkn 335 in January 2009, we limited the UVOT observations to W2 in order to reduce the UVOT filter wheel rotations. The vertical lines in Figure 1 mark the times of the 2007 and 2009 *XMM-Newton* observations. The XRT count rates, hardness ratios and UVOT magnitudes for these light curves are summarized in Table 3. Note that the 2009 *XMM-Newton* observation was performed from MJD 54993.3188 to 54996.2500. Compared with the time at which we triggered the 2009 *XMM-Newton* observation, Mkn 335 had become significantly brighter and we found Mkn 335 in an interesting transition into an intermediate flux state. It increased its average XRT count rate from about 0.11 to 0.36 counts s⁻¹ during the time of the *XMM-Newton* observation. The left panel in Figure 2 displays the *Swift* XRT and UVOT W2 light curves before and after the 2009 *XMM-Newton* observation.

When we started monitoring Mkn 335 in May 2007 it was in its historical low state as we reported in Grupe et al. (2007b). However, it became significantly brighter starting from September 2007 and Mkn 335 remained in this intermediate state throughout 2008 (Figure 1). Due to a failure of one of the *Swift* gyros (Grupe et al. 2007b) the UVOT was turned off in September and October 2007. When we started monitoring Mkn 335 again after it came out of the *Swift* sun-constraint in May 2009, we found Mkn 335 back in a low state. This low state was the reason why we triggered our pre-approved *XMM-Newton* observation. Mkn 335 remained in a low state throughout 2009 with a slight increase towards the end of that monitoring episode. In 2010 Mkn 335 has been in a low state for most of the time. After emerging from the *Swift* sun-constraint in May 2011, it shows again a very low state with a *Swift* XRT count rate of 0.08 counts s⁻¹ and even displayed an all-time low state on 2011 August 28 with a count rate of 0.042±0.010 counts s⁻¹ (right panel in Figure 2). However, recently in November 2011 Mkn 335 went into a high state peaking at about 1 count s⁻¹ in the XRT. We therefore changed our observing strategy to a four day cadence. Mkn 335 is now showing a very rapid variability behavior suggesting that it switches into a high state. Currently (January 2012) we are ob-

serving Mkn 335 daily. On 2012 January 11 it displayed the highest XRT count rate measured since January 2009 with 1.3 counts s⁻¹. This X-ray flux is comparable to the 2006 *XMM-Newton* observation shown in Figure 6.

One question regarding a highly variable source like Mkn 335 is, does the spectral shape change with X-ray flux? As we have shown already in Grupe et al. (2008a) the X-ray spectra of Mkn 335 look completely different in the low and high states. The low number of photons in the *Swift* XRT spectra, however, does not allow us to perform a detailed spectral analysis. Still, a hardness ratio provides some clues about the changes in the X-ray spectrum. Figure 3 shows the relation between the count rate and hardness ratio in the *Swift* data¹. Figure 3 suggests that the AGN becomes softer with increasing count rate. This results in a linear correlation coefficient $r_1 = -0.580$ and a Spearman rank order correlation coefficient $r_s = -0.69$ with a Student's T-value $T_s = -9.4$. For both correlations the probability of a random results is $P < 10^{-6}$.

As shown in Figure 1, Mkn 335 also shows variability in all 6 UVOT filters. During the 2009 *XMM-Newton* observation, Mkn 335 appeared to be slightly fainter by about 0.2-0.3 mag in the OM B, U, W1, M2, and W2 Filters (Table 2) compared with the 2007 observation. This is in agreement with the *Swift* UVOT light curves displayed in Figure 1. As listed in Table 3, in the UVOT W2 filter Mkn 335 was about 0.3 magnitudes brighter during the May 2007 X-ray low state compared with the 2009 May/June low-state. UV variability by 0.3 mag is quite common among NLS1s (Grupe et al. 2010). However, Mkn 335 exhibited a remarkable change in W2 in 2010 as displayed in the right panel of Figure 2 when after a sudden drop from 13.25 to 13.54 in September 2010 it became brighter by 0.79 mag over a period of just three and a half months. As shown in the right panel of Figure 2, it shows an even stronger drop between June and September 2011. On 2011 June 11 it reached its brightest UV state seen during our entire *Swift* monitoring campaign with UVW2=12.69 mag. This brightening, how-

¹We define the hardness ratio as $HR = (H-S)/(H+S)$ with S and H being the background corrected counts in the 0.3-1.0 and 1.0-10 keV bands, respectively

ever, was followed by a continuous fading in the W2 filter with the lowest measurement with 13.63 mag on 2011 September 09. This is a drop in W2 by almost 1 magnitude within three months, equivalent to an increase in flux by a factor of 2.5 - one of the strongest changes in the UV observed in our entire AGN sample (Grupe et al. 2010), which even exceeds the UV variability seen in WPVS 007 (Grupe et al. 2007a, 2008b). These drops in the UV flux are extremely rare in NLS1s, which tend to show no or only little UV variability (e.g. Grupe et al. 2010). Now in January 2012 Mkn 335 displays a very high flux in the UV again, peaking on January 18 with a magnitude of 12.67 in UV W2.

Figure 4 displays the relation between the XRT count rate and the UVOT W2 magnitude. This plot shows that Mkn 335 is only found to be faint in the UV when the AGN is faint in X-rays. However, it appears to be bright in the UV independently of the XRT count rate. We found a linear correlation coefficient $r_1 = -0.376$ with a probability $P=0.00020$ of a random result. A Spearman rank order test results in a correlation coefficient $r_s = -0.347$, $T_s = 3.50$ with a probability $P=0.00072$ of a random result. However, there is not a direct correlation with the source being bright in the UV, when also being bright in X-rays. There is a large scatter in the UV W2 magnitude when the AGN appears to be X-ray faint. Note that the faintest and the brightest UV W2 magnitudes are both measured when Mkn 335 has a count rate less than 0.5 count s^{-1} . The large scatter may suggest that the X-ray and UV emission generally do not vary together.

To explore this in more detail, we investigated potential lags in the variability of the *Swift* XRT count rate and the UVOT W2 filter data during the time period 2007 May to 2011 July. Using the Bayesian framework (e.g. Gregory 2005; Albert 2009, for an introduction to Bayesian analysis) we created “synthetic” model count rates from the observed W2 magnitudes. We first transformed the magnitudes into relative fluxes and then applied a Gaussian bandpass filter in order to only retain variability on specific time scales of interest. For every time scale that was tested the same filter was also applied to the observed count rates. The filtered “synthetic” time series was free to be rescaled and shifted in flux, as well as trans-

lated in time. Overall, our model has 4 free parameters: time lag, flux offset and linear scaling factor, and width of the Gaussian used for the timescale of the bandpass filter. We assigned uniform prior probabilities within sensible parameter ranges for all parameters. Assuming normally distributed uncertainties, we then calculated the likelihood of obtaining the observed count rate data, given a particular set of parameter values for our model. Using the nested sampling code MultiNest (Feroz et al. 2009), we calculated the posterior probability distributions for all 4 parameters, as well as the Bayesian evidence. For comparison, we also calculated the Bayesian evidence for a reference model with constant flux (i.e., no information from the W2 magnitudes is used except for the temporal sampling). Our calculations show that the constant flux model is preferred over the model created from the W2 magnitudes. Therefore, we conclude that at present there is not enough evidence for lags between the XRT count rate and W2 filter for Mkn 355. A more detailed description of the method used, and its application to the Mkn 355 data, will be provided in an upcoming paper (Gruberbauer et al., in preparation).

3.2. Short-term variability observed by *XMM-Newton*

Figure 5 shows the *XMM-Newton* EPIC pn count rate and hardness ratio and OM W2 light curves. The pn light curve was binned in 1000s bins. The W2 bins are typically 4400 s as listed in Table 2. Overall, Mkn 335 appeared to be brighter during the 2009 June observation compared with the 2007 July observation (Grupe et al. 2007b). The overall trend is that the AGN becomes softer when the overall count rate increases from the beginning to the end of the *XMM-Newton* observations. Also note that the ‘flares’ appear to be soft. These ‘flares’ show doubling times of roughly 3 hours. This ‘flaring’ is similar to what had been reported by O’Neill et al. (2007) during the 133 ks 2006 *XMM-Newton* high-state observation. The light curve from the 2006 *XMM-Newton* observation is displayed in Figure 6 for comparison.

The *XMM-Newton* 2009 pn light curve shown in Figure 5 suggests a dependence of the hardness ratio and therefore the shape of the X-ray spectrum on count rate. Figure 7 displays the count

rate vs. hardness ratios in the 2009 and 2006 *XMM-Newton* observations in the left and right panels, respectively. Clearly, there is a strong correlation between count rate and hardness ratio in the low-state 2009 observation. A Spearman rank order test results in a correlation coefficient $r_s = -0.73$ with a Student's T- test value $T_s = -15.3$ with a probability of $P < 10^{-4}$ of a random result. However, the high state data from 2006 give a completely different picture. Here we only see a marginal trend that the source becomes softer with increasing count rate. A Spearman rank order test results is $r_s = -0.20$, $T_s = -2.3$, and a probability $P=0.023$.

The *Swift* long-term monitoring data confirm that there is only a strong correlation between the count rate and hardness ratio when the AGN is in the low state. This result is similar to the one found in the *XMM-Newton* data. During the high state (like in the 2006 *XMM-Newton* data) we do not see a dependence of the X-ray spectral shape with X- ray flux.

3.3. X-ray spectral analysis

3.3.1. General remarks

As shown in the previous subsection, Mkn 335 displays a strong dependence of the shape of its X-ray spectrum on its X-ray flux: the X-ray spectrum appears to be harder when Mkn 335 is in a low state and softer when in a bright state. Therefore performing and interpreting the spectral fits to the average data set will be limited. We therefore split the data into 'bright' and 'faint' states, defining 'bright' as phases when the pn count rate was > 4 counts s^{-1} and 'faint' when the count rate was < 3 counts s^{-1} , corresponding to 0.2-10 keV fluxes of 1.6×10^{-14} and 1.2×10^{-14} W m^{-2} , respectively. This results in four spectra, one 'bright' and 'faint' in each of the two orbits. However, most relevant are the spectra of the 'faint' state of the first orbit and the 'bright' state of the second orbit. The other two spectra do not have enough quality to allow detecting significant spectral changes. Therefore for the remainder of the paper we focus on these two epochs of the 2009 observation. The 2009 first orbit 'faint' state and the second orbit 'bright' state data are denoted (I) and (II) in Table 4. In addition, we have also included the low-state spectrum from July 2007

(Grupe et al. 2008a) to our analysis in order to investigate, if and how the overall spectral shape changed over those two years. This spectrum is marked as (III) in Table 4.

In order to see how much the spectra have changed between July 2007 when Mkn 335 was in its low state (Grupe et al. 2008a) and 2009 June, as a first step, we fitted the new data with the 2007 best-fit absorption model. The 2009 first orbit 'faint' and second orbit 'bright' mode were therefore described with a power law model with Galactic and intrinsic partial covering absorption, fixed to the parameters determined for the 2007 low-state data with $N_{H,pc} = 15.1 \times 10^{22}$ cm^{-2} , $f_{pc}=0.94$, and $\alpha_X=1.78$ (Grupe et al. 2008a). The absorber at $z=0$ was fixed to the Galactic value (3.96×10^{20} cm^{-2} ; Dickey & Lockman 1990) which we used for all fits. This fit is shown in the left panel of Figure 8 with the first orbit 'faint' spectrum displayed in black, the 'bright' second orbit spectrum in red and the 2007 low state spectrum in green. Clearly there is a strong deviation of the 2009 data from the neutral partial covering absorber model used for the 2007 spectrum. This result suggests that the absorber and/or the intrinsic continuum spectrum must have changed significantly.

Therefore, in order to start exploring which model can best characterize the observed changes in the spectra, and which models can be safely ruled out, in a second step, we applied some simple spectral models to the new data; and we continue to compare with the previous data (note that those did not have simultaneous *deep* RGS observations). In these models we fix and tie as many parameters as possible and then thaw them in order to study systematically the influence on the spectral fits of each of these parameters. There are strong residuals around 0.5, 0.9 and 6.4 keV which are likely due to well-localized X-ray emission lines and absorption edges. In order to constrain the broadband continuum parameters, we excluded the energy ranges 0.45-0.6, 0.7-1.1, and 5.5-6.7 keV at first from further analysis at this point. These energy bands correspond to the OVII and OVIII emission lines and absorption edges, and the Fe $K\alpha$ emission line complex. This strategy will keep the number of free parameters low and we can focus on the continuum properties first.

3.3.2. Simple spectral models

The results of 5 spectral fits are summarized in Table 4. We start with those simple models that have been routinely applied to essentially all AGN observed so far: a single power law, a broken power law, a power law with soft excess, and a power law with absorption. First of all, we find that a single absorbed power law model does not result in an acceptable fit for any of these spectra. Although a broken power law model does significantly improve the fits, it is not an acceptable model for any of the spectra, either. The same holds true for a power law plus black-body-type soft excess. Therefore, other models are required to describe the data, and we continue with the next most obvious addition: an ionized absorption component.

3.3.3. X-ray continuum fits with partial covering absorber models

As a first step in characterizing the 2009 spectra, we used a power law with neutral partial covering absorber, as we successfully applied it to the 2007 low state data. The absorption column density and the covering fraction were left free to vary. However, this model does not yield acceptable results for the 2009 data, neither when fitting the model to the single spectra, nor when fitting it simultaneously to the 'faint state' of the first orbit and the 'bright state' during the second orbit. The next step was to fit the spectra with an ionized partial covering absorber (*zxipcf* in XSPEC as described by Reeves et al. 2008) and a power law model. As shown in Table 4, the underlying intrinsic continuum spectrum can not be modeled by a single power law and requires an extra component, but addition of a black body component improves the fit. All spectra can be basically fitted with an intrinsic spectrum with the same blackbody temperature and a hard X-ray spectral slope $\alpha_X=1.0$. When all parameters of the ionized partial covering absorber are left free to vary, all 2009 spectra show very similar covering fractions and ionization parameters. If we fix the covering fraction to 51% and the ionization parameter to $\log\xi=1.91$ [10^{-5} W m, ergs s $^{-1}$ cm], then the differences in the spectra are mostly due to changes in the absorption column density of the ionized partial covering absorber.

In a final step, we fitted the 2009 'faint' and

'bright' spectra and the 2007 low state spectrum simultaneously, again with an ionized partial coverer. As shown in Table 4, the 2007 data can be fitted by the ionized partial covering absorber model. However, they are fully consistent with a neutral partial covering absorber model as well.

Given the possible degeneracy of the black-body component and the parameters of the ionized absorber, further modeling and an accurate parameter determination of the absorber parameters, is not possible with the CCD-type spectra discussed here. Therefore, no further modeling is presented here. In fact, our RGS analysis (in prep) suggests that a *multi*-component absorber is preferred to fully characterize the ionized medium. We have demonstrated that fitting the CCD spectrum with a single warm absorber is sufficient and more complex models are not warranted statistically, and would not yield meaningful results.

3.3.4. Fits with Reflection Models

Although the continuum can be fitted by an ionized absorber model quite well, the previous spectral data of Mrk 335 could also be described in terms of the blurred reflection model (e.g. Ross & Fabian 2005). For completeness, here, we briefly show that such a model can also explain the new 2009 data; but we leave a study of the full parameter space of possible models to a dedicated future study (Gallo et al., in preparation).

The initial model is the double reflector model used to interpret the 2007 X-ray weak state of Mrk 335 (Grupe et al. 2008a). The model considered the possibility of having the disc illuminated by two different primary emitters; for example a compact emitter located close to the black hole and a second, more extended corona illuminating the disc at larger distances. In the 2007 low-state the spectrum was described as being reflection dominated where the direct emission from the power law component was significantly suppressed relative to the reflection component. An additional component required in the 2007 low-state was emission from a distant ionized emitter (Grupe et al. 2008a; Longinotti et al. 2008). This was modeled using the vmekal model in XSPEC for a hot, diffuse gas. There were no obvious absorption features in the 2007 spectrum.

Here, the 2007 data and the 2009 data are fitted

together with the model described above. We find that the primary difference in the continuum between 2007 and 2009 is the level of the power law emitter. That is, the power law is more dominant in the 2009 date than in the 2007 low-state. The ionized emitter remains constant in all three spectra and is consistent with being emitted from large distances. The apparent weakness of the emission spectrum in 2009 is attributed to the increased fraction of the power law component in the X-ray band.

Residuals remain in the fit at approximately 1.5 keV. Considering contribution from a warm absorber as is evident in the RGS analysis (Longinotti et al., in preparation) improves the fit. In an upcoming work we are examining this model in much greater detail by considering also the variability of the source during each observation.

3.3.5. Fe K α emission

So far, the energy bins including the Fe K α emission line energy range had been excluded from spectral fitting. The rest frame 6.4 keV Fe K α line is present in all spectra. The width of the line is about $\sigma=140$ eV. In order to determine the flux and equivalent width of the Fe K α line during each observation, we fitted the spectra with a single power law plus redshifted Gaussian line in the 2-10 keV energy range. We found that the line fluxes determined from the 2009 'faint and 'bright' state and 2007 low state spectra are $(9.6\pm 2.2)\times 10^{-17}$ W m $^{-2}$, $(12.9\pm 2.4)\times 10^{-17}$ W m $^{-2}$, and $(13.2\pm 3.3)\times 10^{-17}$ W m $^{-2}$, respectively. These fluxes suggest that the line has been constant regardless in which state the AGN is. The equivalent widths were 220 ± 75 , 200 ± 60 , and 310 ± 110 eV, respectively. The values for the narrow Fe K α line are very similar when the reflection model is applied to the data.

4. Discussion and Conclusions

We presented the results from our long-term monitoring campaign with *Swift* and the short-term light-curve and X-ray spectral analysis of the highly variable NLS1 Mkn 335 using a dedicated, triggered 200 ks observation with *XMM-Newton*. Mkn 335 is one of the best examples of a typically bright AGN that goes through states of

low X-ray fluxes. Another example is the Seyfert 1 PG 0844+349 for which we recently reported on an *XMM-Newton* observation during its deep low X-ray flux state (Gallo et al. 2011). After Mkn 335 was discovered in an extremely low X-ray flux state in May 2007 we discovered in the 20 ks *XMM-Newton* observation from July 2007 that it showed strong soft X-ray emission lines (Grupe et al. 2008a). This observation however was too short to put constraints on the ionized gas properties and to model the continuum shape of the low-state in detail. Therefore, we triggered the deep *XMM-Newton* observation discussed here, which also led to the first detection of narrow absorption lines in Mkn 335 with RGS (Longinotti et al., in preparation).

4.1. Continuum spectrum

As we saw previously for the 2007 low state *XMM-Newton* observations of Mkn 335, partial covering absorber and reflection models yield a similar quality of the spectral fits. The continuum spectrum is highly variable and complex. When Mkn 335 was observed by *XMM-Newton* in June 2009 it varied very fast on timescales of just hours with the spectrum becoming softer with increasing X-ray flux. The 2009 data require that the absorber has to be ionized. Since there were no signs of intrinsic absorption features in the 2000 and 2006 *XMM-Newton* and *Suzaku* data, the presence of the absorber is not permanent, but transient.

How is a partial coverer model consistent with the long-term variability behavior of this NLS1 seen by *Swift*? As shown in Sections 3.1 and 3.2 the X-ray spectra become softer with increasing X-ray flux. At first glance, an increase in flux could mean intrinsically an increase of the accretion rate and therefore luminosity and L/L_{Edd} which would result in a steeper X-ray spectrum (Grupe 2004; Grupe et al. 2010; Shemmer et al. 2008). However, as we have seen from the shape of the X-ray spectrum, this simple picture can not explain the X-ray spectrum which is much more complicated than a simple power law model. A variable partial covering absorber, however, can explain the X-ray light curves seen on long as well and short time scales: When the absorber becomes stronger and the observed X-ray flux lower, the spectrum becomes harder. On the other hand, when the absorber becomes more transparent or even dis-

appears the spectrum becomes soft.

4.2. X-ray variability

As we have shown in Figures 1, 5, and 6 Mkn 335 is highly variable in X-rays on long and short time scales. Our long-term *Swift* monitoring has shown that Mkn 335 varies in X-rays by factors of about 40 even within months. Beside this strong flux variability we also observe a strong spectral variability when the AGN is in a low state. Above a certain threshold we only see X-ray flux variability with no significant changes in the hardness ratio. This behavior appears on short as well as on long time scales (see Figures 3 and 7). Such a behavior has also been reported by Turner et al. (2008, 2011) for NGC 3516. If we assume the partial covering absorber picture, then the spectral changes in the hardness ratio at lower X-ray fluxes can be explained in terms of changes in the absorber properties, such as the column density, covering fraction and ionization parameter.

Indeed, we find that the flux in the Fe K α line is constant, regardless of the state of the AGN. This constant line flux indicates an underlying continuum component that is not variable.

4.3. UV variability

The UV light curve of Mkn 335 is quite remarkable. While NLS1s typically vary by only 0.3 mag in the UV (Grupe et al. 2010), Mkn 335 shows variability by about 1 mag over a time scale of a few months as seen between 2010 September and December and 2011 June and September. (The strongest UV variability we have seen from the *Swift* observations listed in Grupe et al. (2010), was from Seyfert 1.5 galaxies). In Mkn 335, we did not find any clear correlation between the X-ray and UV flux changes during the time period 2007 May to 2011 July. This result may suggest that the changes in the UV flux are not directly linked to changes in the X-ray flux. However, as shown in the *XMM-Newton* short-term light curve Figure 5 the brightening in the OM W2 light curve at the end could be seen as a response to the 'flare' at 225 ks in X-rays. Currently we do not have the temporal resolution to exclude that there is not a direct connection between the UV and X-rays. Our investigation of possible lags between the UV and X-ray emission is certainly affected by

the under-sampling in the *Swift* light curves. As we have seen from the *XMM-Newton* 2009 light curve, Mkn 335 is highly variable even on time scales of hours. Our current *Swift* light curve systematically under-samples these time scales.

4.4. Mkn 335 and AGN in deep minimum X-ray flux states

Mkn 335 is one of the best examples of an AGN that used to be typically in an X-ray bright flux state but then suddenly becomes dramatically fainter. The most extreme of these cases is the Narrow-Line Seyfert 1 galaxy (NLS1) WPVS 007 (Grupe et al. 1995) which dropped by a factor of more than 400 between its ROSAT All-Sky Survey (RASS; Voges et al. 1999) and ROSAT pointed observations about three years later. FUSE UV spectroscopy and *Swift* X-ray observations revealed the presence of strong UV absorption line troughs and a partial covering absorber in X-rays (Leighly et al. 2009; Grupe et al. 2008b). In the case of WPVS 007 our interpretation is that this is a low-luminosity, low-redshift analog of a Broad Absorption Line Quasar (BAL QSO) as suggested by Leighly et al. (2009). Because the black hole mass in WPVS 007 is only a few $10^6 M_{\odot}$, the timescales in this AGN are hundreds of times shorter than in a typical BAL QSO. Mkn 335 could be just another example of such a BAL QSO analogs. As pointed out by (Brandt & Gallagher 2000) and Boroson (2002), BAL QSOs and NLS1s are both AGN with high L/L_{Edd} Eddington ratios, but with significantly different central black hole masses. WPVS 007 as well as Mkn 335 may be the link between these two AGN classes.

4.5. Conclusions

We presented the results from a more than four year long monitoring campaign with *Swift* of the Narrow Line Seyfert 1 galaxy Mkn 335, one of the longest with simultaneous X-ray and UV measurements so far obtained for an AGN. We also presented a 200 ks observation with *XMM-Newton* triggered at low flux state. We found that

- Mkn 335 continues to be highly variable in X-rays on long and short time scales. The total amplitude of variability in count rate in the *Swift* XRT data (peak to dip between 2007 and 2011) is a factor of 24. The lowest

count rate was seen on 2011 August 28 with 0.042 counts s⁻¹ and the highest count rate on 2007 October 18 with 1.277 counts s⁻¹. The fastest doubling timescale we saw from the *XMM-Newton* observation in 2009 was about 2 hours during the first orbit making it one of the most rapidly varying AGN in X-rays.

- The X-ray and UV variability is not strongly correlated. However, during X-ray bright states, the faintest UV states do not occur, while during X-ray low-states the amplitude of UV variability is highest.
- With a variability of about 1 mag in the UV within a few months as seen between 2011 June and September, Mkn 335 is one of the most variable NLS1 known in the UV.
- Its X-ray hardness ratio shows distinct variability patterns in high- and low-state. During the low-states, there is a clear correlation of hardness ratio with count rate. However, this pattern disappears in high-state; hardness ratio is independent of count rate, and occasionally shows some abrupt changes on short time scales.
- Formally, both ionized absorbers and blurred reflectors do provide successful spectral fits to the XMM low-state data.

While the presence of ionized absorption is confirmed by the RGS data (in prep.), the number and the properties of all spectral components present at any given time will be addressed by in-depth follow-up modeling.

Mrk 335 continues to be one of the few AGN which are still bright enough in their low-states for spectral analysis, and therefore hold the best hopes of understanding AGN spectral components, spectral complexity, and mechanisms of variability. We continue to monitor Mrk 335, in order to identify pronounced high- and low-states.

We thank the *Swift* PI Neil Gehrels for approving our various ToO requests to monitor Mkn 335 with *Swift*, and the *XMM-Newton* Science Operations Team for their fast turn around when we requested our 200 ks triggered observation. Many thanks also to the anonymous referee for useful

comments and suggestions. We acknowledge the use of public data from the Swift data archives. This research has made use of the NASA/IPAC Extragalactic Database (NED) which is operated by the Jet Propulsion Laboratory, Caltech, under contract with the National Aeronautics and Space Administration. This research has made use of the XRT Data Analysis Software (XRTDAS) developed under the responsibility of the ASI Science Data Center (ASDC), Italy. SK acknowledges the hospitality of the Aspen Center for Physics, and thanks the participants for discussions on AGN X-ray spectral models. DX and SK acknowledge support from the Chinese National Science Foundation (NSFC) under grant NSFC 10873017. DX also acknowledges support from program 973 (2009CB824800). Swift is supported at PSU by NASA contract NAS5-00136. This research was supported by NASA contracts NNX08AT25G, NNX09AP50G, and NNX09AN12G (D.G.).

REFERENCES

- Albert, J., 2009, “Bayesian Computation with R”, Springer
- Arevalo, P., et al., 2008, MNRAS, 388, 211
- Arnaud, K. A., 1996, ASP Conf. Ser. 101: Astronomical Data Analysis Software and Systems V, 101, 17
- Ballantyne, D.R., Iwasawa, K., & Fabian, A.C., 2001, MNRAS, 323, 506
- Ballo, L., et al., 2008, A&A, 483, 137
- Boroson, T.A., 2002, ApJ, 565, 78
- Brandt, W.N., & Gallagher, S.C., 2000, New Astronomy Review, 44, 461
- Breeveld, A.A., et al., 2010, MNRAS, 406, 1687
- Burrows, D., et al., 2005, Space Science Reviews, 120, 165
- Cardelli, J.A., Clayton, G.C., Mathis, J.S., 1989, ApJ, 345, 245
- Chevalier, L., Collins, S., Dumont, A.-M., Czerny, B., Mouchet, M., Gonçalves, A.C., & Goosmann, R., 2006, A&A, 449, 493
- den Herder, J.W., et al., 2001, A&A, 365, L17

- Dickey, J.M., & Lockman, F.J., 1990, *ARA&A*, 28, 215
- Fabian, A.C., et al., 2002, *MNRAS*, 331, L35
- Fabian, A.C., Miniutti, G., Gallo, L.C., Boller, T., Tanaka, Y., Vaughan, S., & Ross, R.R., 2004. *MNRAS*, 353, 1071
- Fabian, A.C., et al., *Nature*, 459, 540
- Feroz, F., Hobson, M.P., & Bridges, M., 2009, *MNRAS*, 398, 1601
- Gallo, L.C., 2006, *MNRAS*, 368, 479
- Gallo, L.C., Grupe, D., Schartel, N., Komossa, S., Miniutti, G., Fabian, A.C., & Santos-Lleo, M., 2011, *MNRAS*, 412, 161
- Gehrels, N., et al., 2004, *ApJ*, 611, 1005
- George, I.M., Turner, T.J., Yaqoob, T., Netzer, H., Laor, A., Mushotzky, R.F., Nandra, K., & Takahashi, T., 2000, *ApJ*, 531, 52
- Godet, O., et al., *A&A*, 494, 775
- Gondoin, P., Orr, A., Lumb, D., & Santos-Lleo, M., 2002, *A&A*, 388,74
- Gregory, P.C., 2005, *ApJ*, 631, 1198
- Grier C.J., et al., 2012, *ApJ*, 744, L4
- Grupe, D., Beuermann, K., Mannheim, K., Thomas, H.-C., de Martino, D., & Fink, H.H., 1995, *A&A*, 300, L21
- Grupe, D., *AJ*, 127, 1799
- Grupe, D., Thomas, H.-C., & Beuermann, K., 2001, *A&A*, 367, 470
- Grupe, D., Wills, B.J., Leighly, K.M., & Meusinger, H., 2004a, *AJ*, 127, 156 Komossa, S., 2004b, *AJ*, 127, 3161
- Grupe, D., Schady, P., Leighly, K.M., Komossa, S., O'Brien, P.T., & Nousek, J.A., 2007, *AJ*, 133, 1988
- Grupe, D., Komossa, S., & Gallo, L., 2007b, *ApJ*, 668, L111
- Grupe, D., Komossa, S., Gallo, L.C., Fabian, A., Larsson, J., Pradhan, A.K., Xu, D., & Miniutti, G., 2008a, *ApJ*, 681, 982
- Grupe, D., Leighly, K.M., & Komossa, S., 2008b, *AJ*, 136, 2343
- Grupe, D., Komossa, S., Leighly, K.M., & Page, K.L., 2010, *ApJS*, 187,64
- Halpern, J.P., 1982, PhD thesis, Harvard University
- Hill, J.E., et al., 2004, *SPIE*, 5165, 217
- Jansen, F., et al., 2001, *A&A*, 365, L1
- Larsson, J., Miniutti, G., Fabian, A.C., Miller, J.M., Reynolds, C.S., & Ponti, G., 2008, *MNRAS*, 384, 1316
- Leighly, K.M., 1999, *ApJS*, 125, 317
- Leighly, K.M., Halpern, J.P., Jenkins, E.B., Grupe, D., Choi, J., & Prescott, K.B., 2007, *ApJ*, 663, 103
- Leighly, K.M., Hamann, F., Casebeer, D.A., & Grupe, D., 2009, *ApJ*, 701, 176
- Longinotti, A.L., Sim, S.A., Nandra, K., & Cappi, M., 2007a, *MNRAS*, 374, 237
- Longinotti, A.L., Sim, S.A., Nandra, K., Cappi, M., & O'Neill, P., 2007b, *ASP Conf. Series*, Vol. 373, proceedings of the conference held 16-21 October, 2006 at Xi'an Jiaotong University, Xi'an, China. Edited by Luis C. Ho and Jian-Min Wang, p.341
- Longinotti, A.L., Nucita, A., Santos-Lleo, M., & Guainazzi, M., 2008, *A&A*, 484, 311
- Longinotti, A.L., Bianchi, S., Ballo, L., de la Calle, I., & Guainazzi, M., 2009, *MNRAS*, 394, L1
- Mason, K.O., et al., 2001, *A&A*, 365, L36
- Merloni, A., Malzac, J., Fabian, A.C., & Ross, R.R., 2006, *MNRAS*, 370, 1699
- Miller, L., Turner, T.J., Reeves, J.N., George, I.M., Kraemer, S.B., & Wingert, B., 2007, *A&A*, 463, 131
- Miller L., Turner, T.J., & Reeves, J.N., 2008, *A&A*, 483, 437
- Miller L., Turner, T.J., & Reeves, J.N., 2009, *MNRAS*, 399, L96

- Miniutti, G., Fabian, A.C., Brandt, W.N., Gallo, L.C., & Boller, T., 2009, MNRAS, 396, L85
- Nahar, S.N., et al., 2011, Phys Rev A, 83, 053417
- Nandra, K., & Pounds, K.A., 1994, MNRAS, 268, 405
- O’Neill, P.M., Nandra, K., Cappi, M., Longinotti, A.L., & Sim, S.A., 2007, MNRAS, 381, L94
- Peterson, B.M., et al., 2004, ApJ, 613, 682
- Poole, T.S., et al., 2008, MNRAS, 383, 627
- Pounds, K.A., Stanger, V.J., Turner, T.J., King, A.R., & Czerny, B., 1987, MNRAS, 224, 443
- Reeves, J., et al., 2008, MNRAS, 385, L108
- Risaliti, G., et al., 2009, MNRAS, 393, L1
- Roming, P.W.A., et al., 2005, Space Science Reviews, 120, 95
- Roming, P.W.A., et al., 2009, ApJ, 690, 163
- Ross, R.R., & Fabian, A.C., 2005, MNRAS, 358, 211
- Schartel, N., et al., 2007, A&A, 474, 431
- Schartel, N., Rodríguez- PAscual, P.M., Santos-Lleó, M., Jiménez-Bailón, E., Ballo, L., Piconcelli, E., 2010, A&A, 512, 75
- Shemmer, O., Brandt, W.N., Netzer, H., Maiolino, R., & Kaspi, S., 2008, ApJ, 682, 81
- Schlegel, D. J., Finkbeiner, D. P., & Davis, M. 1998, ApJ, 500, 525
- Strüder, L., et al., 2001, A&A, 365, L18
- Tanaka, Y., et al., 1995, Nature, 375, 659
- Tananbaum, H., Peters, G., Forman, W., Giacconi, R., Jones, C., & Avni, Y., 1978, ApJ, 223, 74
- Turner, T.J., et al., 1993, ApJ, 407, 556
- Turner, M.J., et al., 2001, A&A, 365, L27
- Turner, T.J., Miller, L., Reeves, J.N., & Kraemer, S.B., 2007, A&A, 475, 121
- Turner, T.J., Reeves, J.N., Kraemer, S.B., & Miller, L., 2008, A&A, 483, 161
- Turner, T.J., Miller, L., Kraemer, S.B., & Reeves, J.N., 2011, ApJ, 733, 48
- Turner, T.J., & Miller, L., 2009, A&AR, 17, 47
- Vignali, C., et al., 2008, MNRAS, 388, 761
- Voges, W., Aschenbach, B., Boller, T., et al., 1999, A&A, 349, 389

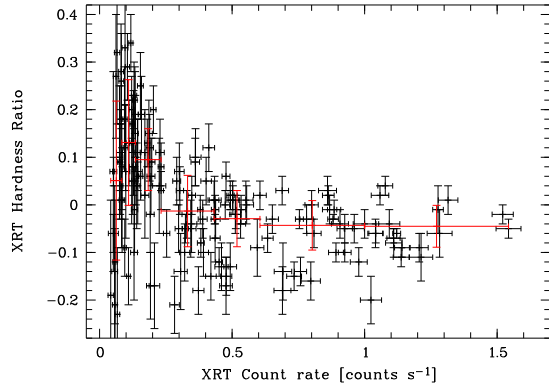


Fig. 3.— Count rate vs. hardness ratio during the *Swift* observations. The red crosses correspond to bins in count rate containing 25 measurements and the mean hardness ratio and standard deviation in that bin.

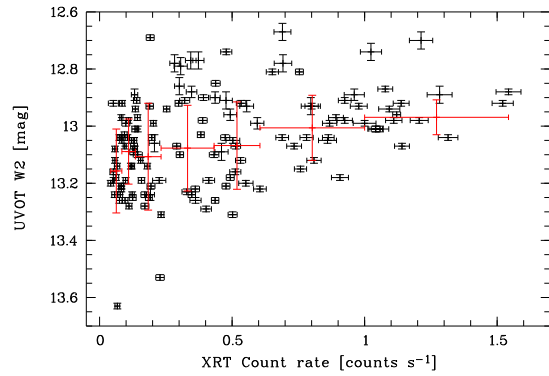


Fig. 4.— *Swift* XRT Count rate vs. UVOT W2 magnitude. The red crosses correspond to bins in count rate containing 25 measurements and the mean UVOT W2 magnitude and standard deviation in that bin.

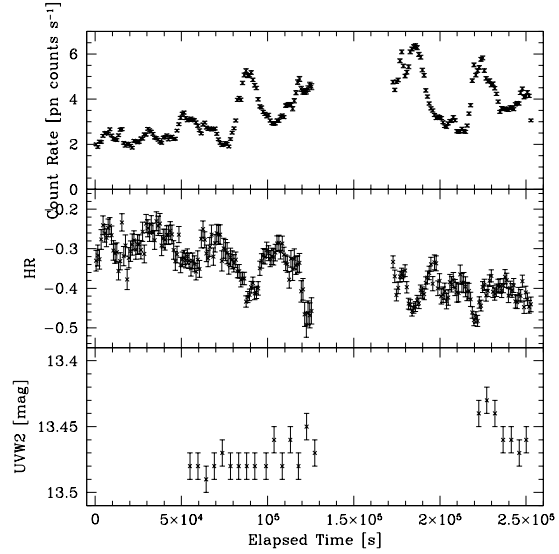


Fig. 5.— *XMM-Newton* pn and OM W2 light curves of Mkn 335 during the 2009 observation.

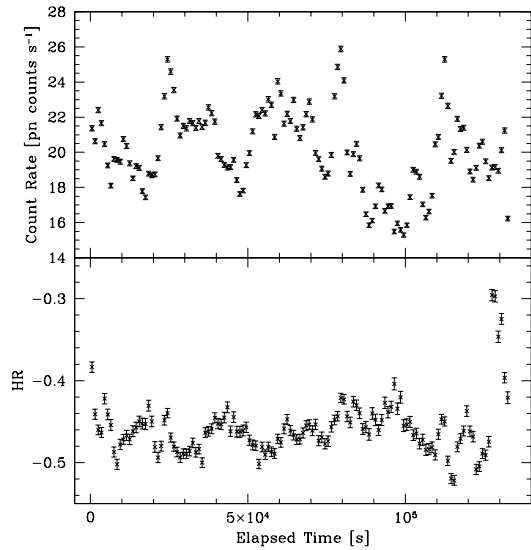


Fig. 6.— *XMM-Newton* pn light curves of Mkn 335 during the 2006 observation.

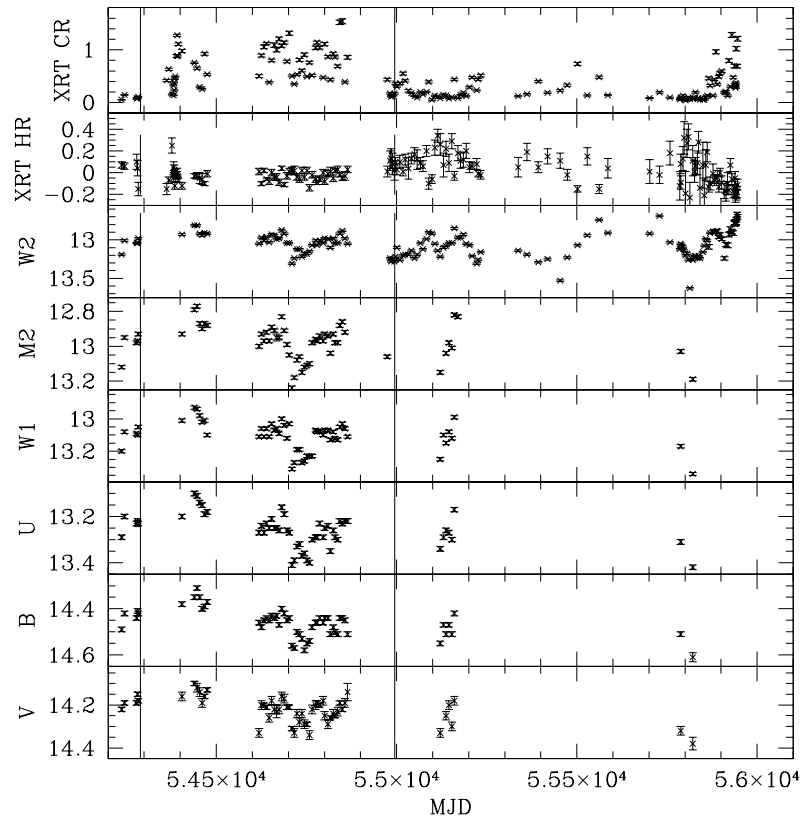


Fig. 1.— *Swift* XRT and UVOT light curves of Mkn 335. The vertical lines at MJD 54290 and 54995 mark the times of the *XMM-Newton* observations in July 2007 and June 2009. The beginning of the light curve is 2007 May 17.

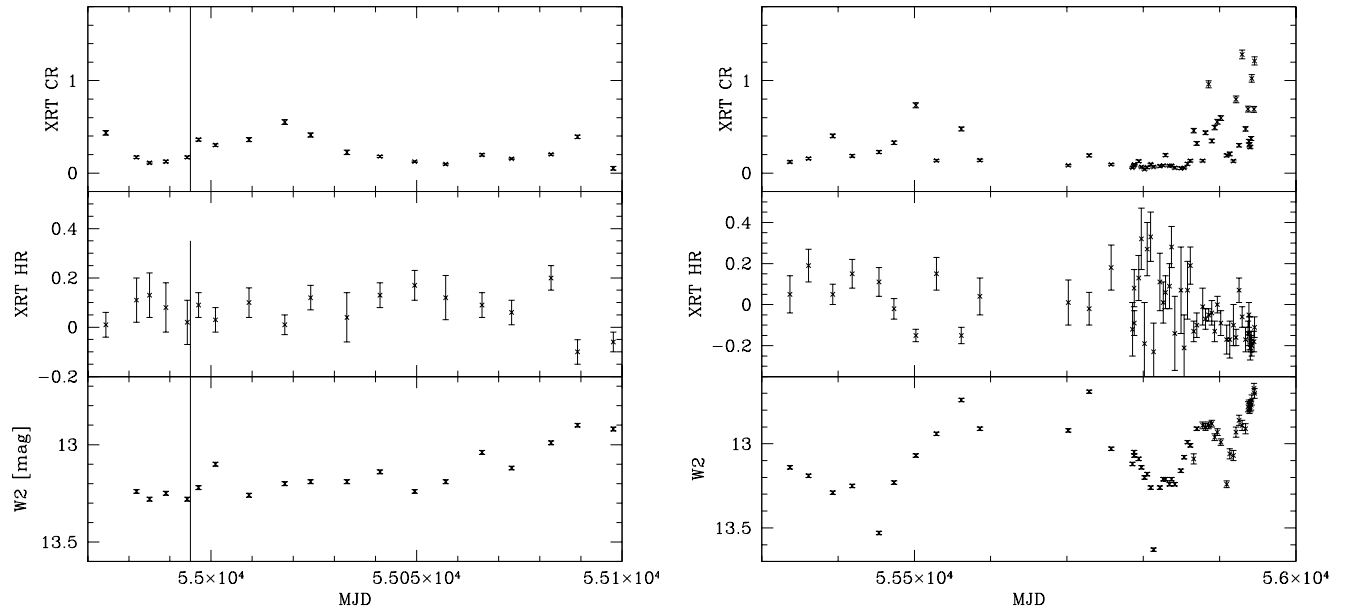


Fig. 2.— Zoom-in of the *Swift* XRT and UVOT W2 light curves of Mkn 335. The left panel displays the *Swift* observations before and shortly after the 2009 *XMM-Newton* observation. The vertical line at MJD 54995 marks the time of the *XMM-Newton* observation in June 2009. The beginning of this light curve is 2009 May 23. The right panel shows the light curves in 2010 and 2011

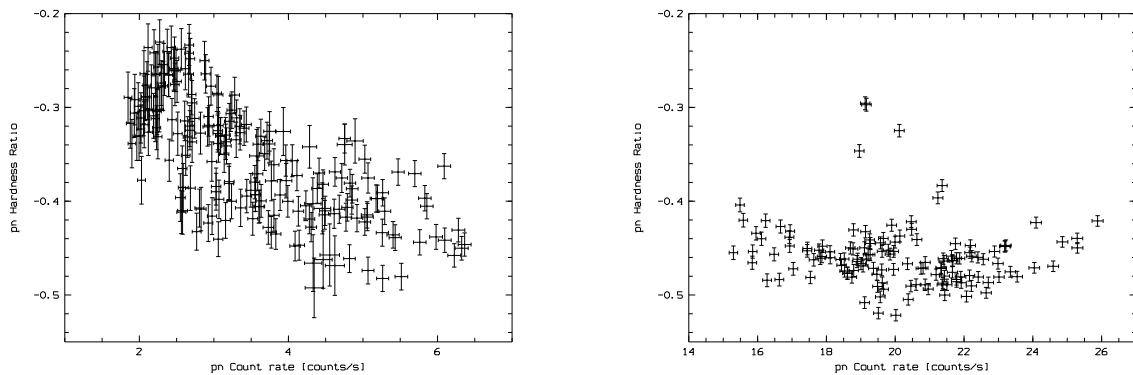


Fig. 7.— Count rate vs. Hardness ratio of the 2009 (left) and 2006 (right) *XMM-Newton* observations.

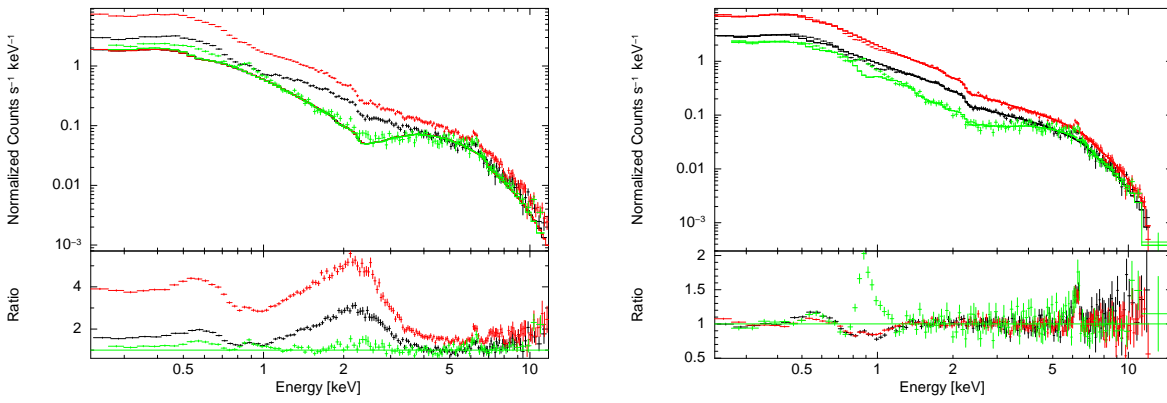


Fig. 8.— *XMM-Newton* 2009 first orbit 'faint state', second orbit 'bright state' and the pn 2007 low state data of Mkn 335. The data are displayed in black, red and green, respectively. In the left panel the spectra were modeled by a neutral partial covering absorber model using the parameters as given in Grupe et al. (2008a); $N_{\text{H,pc}} = 15.1 \times 10^{22} \text{ cm}^{-2}$, $f_{\text{pc}}=0.94$, $\alpha_{\text{X}}=1.78$. In the right panel the spectra were fitted with an ionized partial covering absorber and an underlying black body plus power law spectrum as listed in Table 4.

TABLE 1—Continued

ObsID	Segment	T-start ¹		T-stop ¹	MJD ²	T _{XRT} ³	T _V ³	T _B ³	T _U ³	T _{UVW1} ³	T _{UVM2} ³	T _{UVW2} ³	
	066	2009-11-18	10:43	2009-11-18	15:27	55153.545	2010	160	160	160	320	471	640
	067	2009-11-25	11:15	2009-11-25	13:07	55160.508	1949	161	161	161	322	429	645
	068	2009-12-04	21:40	2009-12-04	05:47	55170.072	2455	1735	690
	069	2009-12-11	23:56	2009-12-12	10:05	55177.208	1799	2044
	070	2009-12-20	00:41	2009-12-20	12:28	55185.274	2198	2186
	071	2009-12-28	01:25	2009-12-28	03:23	55193.100	2049	2038
	072	2010-01-05	21:32	2010-01-05	23:25	55201.937	1956	1949
	073	2010-01-13	00:01	2010-01-13	12:57	55209.270	2619	3036
	074	2010-01-25	21:41	2010-01-25	23:37	55221.944	2218	2200
	075	2010-01-29	22:08	2010-01-30	09:38	55226.162	2622	2596
	076	2010-02-06	03:36	2010-02-06	05:24	55233.188	1907	1914
35755	029	2010-05-21	02:12	2010-05-21	02:32	55337.098	1140	1149
	030	2010-06-14	08:59	2010-06-14	09:20	55361.382	1206	1203
	031	2010-07-16	01:01	2010-07-16	02:48	55393.080	1209	1209
	033	2010-08-10	12:57	2010-08-10	14:46	55418.577	1279	1279
	035	2010-09-14	16:05	2010-09-14	16:22	55453.676	1082	1082
	036	2010-10-04	09:45	2010-10-04	10:05	55473.413	1257	1251
	037	2010-11-01	21:53	2010-11-01	22:15	55501.920	1343	1339
	038	2010-11-29	01:34	2010-11-29	01:58	55529.074	1362	1361
	040	2010-12-31	15:46	2010-12-31	16:07	55561.665	1263	1266
	042	2011-01-24	22:43	2011-01-24	23:01	55585.953	1065	1049
	044	2011-05-20	18:12	2011-05-20	18:31	55701.765	1097	1102
	045	2011-06-17	01:31	2011-06-17	01:48	55729.069	977	983
	046	2011-07-15	23:05	2011-07-15	23:22	55757.968	982	987
	047	2011-08-12	15:48	2011-08-12	20:23	55785.754	1096	1088
	048	2011-08-14	22:15	2011-08-14	23:42	55787.957	1962	132	133	133	619	383	530
	049	2011-08-15	03:24	2011-08-15	06:22	55788.230	2943	2908
	050	2011-08-20	21:19	2011-08-20	21:34	55793.894	859	856
	051	2011-08-24	10:22	2011-08-24	13:44	55797.502	767	790
	052	2011-08-28	13:34	2011-08-28	13:50	55801.571	1006	1001
	053	2011-09-01	03:06	2011-09-01	22:14	55805.135	1094	1083
	054	2011-09-05	15:50	2011-09-05	16:08	55809.666	1025	1025
	055	2011-09-09	05:12	2011-09-09	15:10	55813.425	1058	1085
	056	2011-09-17	15:39	2011-09-17	15:52	55821.657	731	61	61	61	122	185	243
	057	2011-09-22	00:03	2011-09-22	06:37	55826.139	1140	1202
	058	2011-09-25	00:10	2011-09-25	00:26	55829.012	934	944
	059	2011-09-30	06:45	2011-09-30	07:05	55834.288	1145	1159
	060	2011-10-03	00:39	2011-10-03	00:59	55837.034	1215	1201
	061	2011-10-07	07:21	2011-10-07	07:37	55841.312	896	907
	062	2011-10-15	04:32	2011-10-15	06:36	55849.235	849	840
	063	2011-10-19	10:05	2011-10-19	10:20	55853.425	867	862
	064	2011-10-23	19:55	2011-10-23	20:04	55857.833	535	550
	065	2011-10-27	12:05	2011-10-27	12:24	55861.510	1015	1090
	066	2011-10-31	22:16	2011-10-31	22:33	55865.934	974	969
	067	2011-11-04	22:33	2011-11-04	22:50	55869.945	1016	1012
	068	2011-11-12	16:43	2011-11-12	17:00	55877.702	984	989
	069	2011-11-16	13:42	2011-11-16	14:05	55881.579	1256	1328
	070	2011-11-20	15:17	2011-11-20	17:01	55885.673	1033	1029
	071	2011-11-24	19:07	2011-11-24	19:24	55889.802	1001	1011
	072	2011-11-28	11:24	2011-11-28	11:41	55893.481	989	977
	073	2011-12-02	03:18	2011-12-02	03:35	55897.144	989	984
	074	2011-12-06	13:26	2011-12-06	15:15	55901.598	1351	1336
	076	2011-12-14	02:45	2011-12-14	03:02	55909.121	976	973
	077	2011-12-18	02:56	2011-12-18	07:49	55913.224	807	812
	078	2011-12-23	00:03	2011-12-23	02:14	55918.048	1091	1310
	079	2011-12-26	11:45	2011-12-26	12:01	55921.495	939	945
	080	2011-12-30	11:51	2011-12-30	13:34	55925.530	1091	1076
	081	2012-01-03	12:30	2012-01-03	17:24	55929.623	1226	243
	082	2012-01-07	20:37	2012-01-07	20:54	55933.864	996	1002
	083	2012-01-11	04:53	2012-01-11	05:10	55937.209	999	999
	084	2012-01-12	07:45	2012-01-12	08:03	55938.329	1029	1033
	085	2012-01-13	03:03	2012-01-13	03:18	55939.132	844	852
	086	2012-01-14	01:28	2012-01-14	01:45	55940.067	969	973
	087	2012-01-15	04:45	2012-01-15	05:02	55941.204	976	985
	088	2012-01-16	03:12	2012-01-16	03:29	55942.139	976	973
	090	2012-01-18	22:43	2012-01-18	23:01	55944.953	1036	1042
	091	2012-01-19	19:28	2012-01-19	19:45	55945.817	967	974

¹Start and End times are given in UT

²The MJD marks the middle of the observation

³Observing time given in s

TABLE 2
XMM-Newton OBSERVATION LOG OF MKN 335

Filter/Detector	T-start ¹	T-end ¹	T-exp ²	Mag ³	2007 Mag ⁴
pn	2009-06-11 07:39	2009-06-12 19:54	114784		
MOS-1	2009-06-11 07:16	2009-06-12 19:57	131920		
MOS-2	2009-06-11 07:17	2009-06-12 19:57	131972		
pn	2009-06-13 07:31	2009-06-14 05:56	80344		
MOS-1	2009-06-13 07:08	2009-06-14 06:00	82257		
MOS-2	2009-06-13 07:08	2009-06-14 06:00	82249		
OM V	2009-06-11 07:25	2009-06-11 08:38	4400	14.47±0.01	
OM U	2009-06-11 08:43	2009-06-11 09:57	4400	13.65±0.01	13.36±0.01
OM B	2009-06-11 10:02	2009-06-11 11:15	4400	14.73±0.01	14.50±0.01
OM W1	2009-06-11 11:20	2009-06-11 12:34	4400	13.34±0.01	13.09±0.01
OM W1	2009-06-11 12:39	2009-06-11 13:52	4400	13.34±0.01	
OM W1	2009-06-11 14:26	2009-06-11 15:41	4400	13.34±0.01	
OM M2	2009-06-11 15:46	2009-06-11 16:59	4400	13.37±0.01	13.14±0.01
OM M2	2009-06-11 17:04	2009-06-11 18:17	4400	13.39±0.01	
OM M2	2009-06-11 18:22	2009-06-11 19:36	4400	13.40±0.01	
ON M2	2009-06-11 20:59	2009-06-11 22:13	4400	13.21±0.01	
OM W2	2009-06-11 22:18	2009-06-11 23:31	4400	13.48±0.01	13.22±0.01
OM W2	2009-06-11 23:36	2009-06-12 00:50	4400	13.48±0.01	
OM W2	2009-06-12 00:55	2009-06-12 02:08	4400	13.49±0.02	
OM W2	2009-06-12 02:13	2009-06-12 03:27	4400	13.48±0.01	
OM W2	2009-06-12 03:32	2009-06-12 04:45	4400	13.47±0.01	
OM W2	2009-06-12 04:50	2009-06-12 06:03	4400	13.48±0.01	
OM W2	2009-06-12 06:09	2009-06-12 07:22	4400	13.48±0.01	
OM W2	2009-06-12 07:27	2009-06-12 08:40	4400	13.48±0.01	
OM W2	2009-06-12 08:45	2009-06-12 09:59	4400	13.48±0.01	
OM W2	2009-06-12 10:34	2009-06-12 11:47	4400	13.48±0.01	
OM W2	2009-06-12 11:52	2009-06-12 13:06	4400	13.46±0.01	
OM W2	2009-06-12 13:11	2009-06-12 14:24	4400	13.48±0.01	
OM W2	2009-06-12 14:29	2009-06-12 15:43	4400	13.46±0.01	
OM W2	2009-06-12 15:48	2009-06-12 17:01	4400	13.48±0.01	
OM W2	2009-06-12 17:06	2009-06-12 18:20	4400	13.45±0.01	
OM W2	2009-06-12 18:25	2009-06-12 19:30	3920	13.47±0.01	
OM V	2009-06-13 07:17	2009-06-13 08:30	4400	14.48±0.01	
OM U	2009-06-13 08:35	2009-06-13 09:48	4400	13.67±0.01	
OM B	2009-06-13 09:54	2009-06-13 11:07	4400	14.73±0.01	
OM W1	2009-06-13 11:12	2009-06-13 12:25	4400	13.35±0.01	
OM W1	2009-06-13 12:30	2009-06-13 13:44	4400	13.35±0.01	
OM M2	2009-06-13 14:19	2009-06-13 15:32	4400	13.43±0.01	
OM M2	2009-06-13 15:37	2009-06-13 16:50	4400	13.38±0.01	
OM M2	2009-06-13 16:56	2009-06-13 18:09	4400	13.40±0.01	
OM M2	2009-06-13 18:14	2009-06-13 19:28	4400	13.38±0.01	
OM M2	2009-06-13 19:33	2009-06-13 20:46	4400	13.37±0.01	
OM W2	2009-06-13 20:51	2009-06-13 22:41	4400	13.44±0.01	
OM W2	2009-06-13 22:10	2009-06-13 23:23	4400	13.43±0.01	
OM W2	2009-06-13 23:28	2009-06-14 00:42	4400	13.44±0.01	
OM W2	2009-06-14 00:47	2009-06-14 02:00	4400	13.46±0.01	
OM W2	2009-06-14 02:05	2009-06-14 03:18	4400	13.46±0.01	
OM W2	2009-06-14 03:23	2009-06-14 04:37	4400	13.47±0.01	
OM W2	2009-06-14 04:42	2009-06-14 05:33	3100	13.46±0.01	

¹Start and end times are given in UT

²Exposure times given in s

³Observed magnitudes not corrected for Galactic reddening at the position of Mkn 335

⁴The 2007 OM data are listed here as a comparison to the 2009 observations. For the exact observing time we refer to Grupe et al. (2008a).

TABLE 3—Continued

ObsID	Segment	MJD	XRT CR	XRT HR	V	B	U	UVW1	UVM2	UVW2
	066	55153.545	0.105±0.008	+0.29±0.07	14.30±0.02	14.51±0.01	13.30±0.01	13.12±0.01	13.01±0.01	13.04±0.01
	067	55160.508	0.438±0.017	-0.03±0.04	14.18±0.02	14.42±0.01	13.17±0.01	12.99±0.01	12.82±0.01	12.85±0.01
	068	55170.072	0.082±0.006	+0.18±0.07	12.83±0.01	12.97±0.01
	069	55177.208	0.143±0.010	+0.11±0.07	12.97±0.01
	070	55185.274	0.189±0.014	+0.12±0.07	12.93±0.01
	071	55193.100	0.121±0.010	+0.20±0.07	13.05±0.01
	072	55201.937	0.291±0.015	+0.05±0.05	13.07±0.01
	073	55209.270	0.477±0.015	+0.06±0.03	13.21±0.01
	074	55221.944	0.232±0.011	+0.08±0.05	13.31±0.01
	075	55226.162	0.436±0.014	-0.01±0.03	13.26±0.01
	076	55233.188	0.512±0.021	-0.02±0.04	13.16±0.01
35755	029	55337.098	0.121±0.011	+0.05±0.09	13.14±0.01
	030	55361.381	0.158±0.012	+0.19±0.08	13.19±0.01
	031	55393.080	0.402±0.020	+0.05±0.05	13.29±0.01
	033	55418.577	0.186±0.013	+0.15±0.07	13.25±0.01
	035	55453.676	0.228±0.016	+0.11±0.07	13.53±0.01
	036	55473.413	0.330±0.018	-0.02±0.05	13.23±0.01
	037	55501.920	0.734±0.028	-0.15±0.03	13.07±0.01
	038	55529.074	0.135±0.011	+0.15±0.08	12.94±0.01
	040	55561.665	0.478±0.021	-0.16±0.04	12.74±0.01
	042	55585.953	0.140±0.012	+0.04±0.09	12.91±0.01
	044	55701.765	0.085±0.010	+0.01±0.10	12.92±0.01
	045	55729.069	0.191±0.015	-0.02±0.08	12.69±0.01
	046	55757.968	0.094±0.010	+0.18±0.11	13.03±0.01
	047	55785.754	0.058±0.008	-0.12±0.13	13.03±0.01
	048	55787.957	0.084±0.008	+0.08±0.09	14.32±0.02	14.51±0.01	13.31±0.01	13.17±0.01	13.03±0.01	13.05±0.01
	049	55788.203	0.095±0.006	-0.09±0.06	13.07±0.01
	050	55793.894	0.128±0.014	+0.13±0.11	13.09±0.01
	051	55797.502	0.066±0.010	+0.32±0.15	13.14±0.01
	052	55801.571	0.042±0.010	-0.19±0.20	13.20±0.01
	053	55805.135	0.062±0.010	+0.27±0.13	13.18±0.01
	054	55809.666	0.098±0.011	+0.33±0.11	13.26±0.01
	055	55813.425	0.067±0.009	-0.23±0.13	13.63±0.01
	056	55821.657	0.076±0.011	+0.12±0.14	14.38±0.03	14.61±0.02	13.42±0.01	13.34±0.01	13.19±0.02	13.26±0.01
	057	55826.139	0.083±0.009	+0.01±0.11	13.21±0.01
	058	55829.012	0.194±0.015	+0.06±0.08	13.21±0.01
	059	55834.288	0.079±0.009	+0.09±0.11	13.24±0.01
	060	55837.034	0.081±0.009	+0.27±0.10	13.21±0.01
	061	55841.312	0.057±0.011	-0.14±0.18	13.24±0.01
	062	55849.235	0.052±0.013	+0.07±0.21	13.16±0.01
	063	55853.425	0.058±0.009	-0.22±0.15	13.04±0.03
	064	55857.833	0.099±0.015	+0.07±0.14	12.99±0.01
	065	55861.510	0.134±0.012	+0.19±0.09	13.01±0.01
	066	55865.934	0.460±0.025	-0.13±0.05	13.09±0.03
	067	55869.945	0.321±0.019	-0.10±0.06	12.91±0.01
	068	55877.702	0.132±0.012	-0.01±0.09	12.89±0.02
	069	55881.578	0.436±0.019	-0.07±0.05	12.90±0.02
	070	55885.673	0.961±0.038	-0.05±0.03	12.89±0.02
	071	55889.802	0.347±0.020	-0.04±0.06	12.88±0.02
	072	55893.481	0.493±0.024	-0.13±0.05	12.96±0.02
	073	55897.144	0.555±0.026	-0.00±0.04	12.93±0.02
	074	55901.598	0.595±0.025	-0.09±0.06	12.99±0.02
	076	55909.121	0.192±0.015	-0.17±0.07	13.24±0.02
	077	55913.224	0.207±0.020	-0.17±0.09	13.06±0.03
	078	55918.048	0.130±0.013	-0.10±0.10	13.07±0.03
	079	55921.495	0.797±0.036	-0.16±0.04	12.93±0.03
	080	55925.530	0.301±0.018	+0.07±0.06	12.86±0.03
	081	55929.623	1.283±0.047	-0.06±0.05	12.89±0.03
	082	55933.864	0.477±0.024	-0.17±0.06	12.91±0.03
	083	55937.209	0.692±0.033	-0.14±0.06	12.78±0.03
	084	55938.329	0.344±0.020	-0.05±0.06	12.77±0.03
	085	55939.132	0.306±0.025	-0.14±0.08	12.79±0.03
	086	55940.067	0.283±0.018	-0.21±0.06	12.78±0.03
	087	55941.204	0.373±0.021	-0.18±0.05	12.77±0.03
	088	55942.139	1.024±0.040	-0.20±0.05	12.74±0.03
	090	55944.953	0.690±0.032	-0.18±0.05	12.67±0.03
	091	55945.817	1.213±0.044	-0.11±0.05	12.70±0.03

¹Magnitude corrected for reddening with $E_{B-V}=0.037$ given by Schlegel et al. (1998). The errors given in this table are statistical errors

TABLE 4

RESULTS OF THE SPECTRAL FITS TO THE 'FAINT' AND 'BRIGHT' STATE *XMM-Newton* PN DATA OF MKN 335 DURING THE FIRST AND SECOND ORBIT.

Spectrum ¹	Model ²	$\alpha_{X,soft}$	E_{break}	$\alpha_{X,hard}$	T_{BB} ³	$N_{H,pc}$ ⁴	f_{pc}	$\log(\xi)$ ⁵	χ^2/ν
(I)	powl	1.36±0.01	—	—	—	—	—	—	4071/117
	bknpo	1.74±0.02	1.27±0.03	0.52±0.02	—	—	—	—	198/115
	bb + po	—	—	0.52±0.02	99±2	—	—	—	209/115
	zpcfabs * po	1.65±0.01	—	—	—	5.1±0.2	0.78±0.01	—	516/115
	zpcfabs * (bb + po)	—	—	0.77 ^{+0.06} _{-0.12}	97±2	3.7±1.0	0.33 ^{+0.05} _{-0.13}	—	191/113
	zxipcf * po	1.18±0.01	—	—	—	5.75±0.30	1.00 ⁶	2.24±0.02	255/114
	zxipcf * (bb+po)	—	—	0.92 ^{+0.05} _{-0.10}	110 ⁺³ ₋₅	10.5±1.5	0.51 ^{+0.05} _{-0.09}	1.91 ^{+0.05} _{-0.08}	154/112
(II)	powl	1.55±0.01	—	—	—	—	—	—	6749/135
	bknpo	1.86±0.01	1.34±0.02	0.73±0.02	—	—	—	—	338/133
	bb + po	—	—	0.75±0.01	97±2	—	—	—	511/133
	zpcfabs * po	1.79±0.01	—	—	—	5.5±0.2	0.76±0.01	—	838/133
	zpcfabs * (bb + po)	—	—	1.11 ^{+0.04} _{-0.08}	94±1	5.3 ^{+0.6} _{-0.5}	0.43 ^{+0.03} _{-0.08}	—	429/131
	zxipcf * po	1.35±0.01	—	—	—	5.95±0.20	1.00 ⁶	2.30±0.02	439/132
	zxipcf * (bb+po)	—	—	1.12±0.02	106 ⁺³ ₋₂	13.1±1.2	0.51 ⁷	1.91 ⁷	245/132
(III)	zpcfabs * (bb + po)	—	—	1.44±0.12	105 ⁺⁷ ₋₆	13.5 ^{+1.1} _{-1.0}	0.90±0.02	—	136/87
	zxipcf *(bb+po)	—	—	0.94 ^{+0.08} _{-0.09}	113 ⁺¹⁰ ₋₈	22.4 ^{+4.2} _{-1.6}	0.87 ^{+0.02} _{-0.03}	2.06±0.05	132/86
(I) + (II)	zpcfabs * (bb + po)	—	—	0.97±0.05	95±3	5.6 ^{+1.0} _{-0.7}	0.31±0.04	—	647/246
	zxipcf * (bb+po)	—	—	1.17 ^{+0.04} _{-0.03}	110±3	6.0 ^{+0.6} _{-0.5}	0.68±0.02	1.23 ^{+0.11} _{-0.24}	406/244
(I) + (II) + (III)	zpcfabs * (bb+po)	—	—	1.04±0.05	96±3	4.1±0.4 5.3 ^{+1.0} _{-0.7} 12.8±1.2	0.53±0.03 0.37±0.04 0.81±0.02	—	823/334
	zxipcf * (bb+po)	—	—	1.17 ^{+0.04} _{-0.03}	110±3	6.0 ^{+0.6} _{-0.5} 13.5±1.0 22.3 ^{+3.9} _{-1.5}	0.68 ^{+0.02} _{-0.01} 0.57±0.03 0.88±0.02	1.23 ^{+0.12} _{-0.21} 1.91±0.03 2.05±0.05	535/329

¹Spectra: (I) 2009, Orbit 1, faint; (II) 2009, Orbit 2, bright; (III) 2007

²Spectra models: powl: single power law; bknpo: broken power law; bb: black body; zpcfabs: redshifted neutral partial covering absorber, zxipcf: ionized redshifted partial covering absorber; Note that all models are fitted with the absorption model wabs with the column density fixed to the Galactic value of $3.96 \times 10^{20} \text{ cm}^{-2}$ taken from Dickey & Lockman (1990). For all models we excluded the energy ranges 0.45-0.6, 0.7-1.1, and 5.5-6.7 keV.

³The black body temperature T_{BB} is given in units of eV.

⁴The column density of the ionized partial covering absorber is given in units of 10^{22} cm^{-2} .

⁵The ionization parameter ξ is given in units 10^{-5} W m , or $\text{ergs s}^{-1} \text{ cm}$.

⁶The covering fraction of the ionized absorber pegged.

⁷Covering fraction and ionization parameter fixed to the values of the low state. When left as free parameters $\log \xi$ results in the same value, but f_{pc} is not constrained.